Polymer 186 (2020) 122048

Contents lists available at ScienceDirect

Polymer

journal homepage: http://www.elsevier.com/locate/polymer

CarNit4 – A new polymeric energetic material based on poly (1,5-tetrazolediyl)

Sergey V. Bondarchuk

Department of Chemistry and Nanomaterials Science, Bogdan Khmelnitsky Cherkasy National University, blvd. Shevchenko 81, 18031, Cherkasy, Ukraine

ARTICLE INFO

Keywords:
Nitrogen-rich heterocycles
Energetic polymers
DFT calculations

ABSTRACT

In this paper, a theoretical design and characterization of a novel nitrogen-rich polymeric material (CarNit4) based on 1,5-tetrazolediyl unit was performed using density functional theory. The theoretical analysis includes crystal structure prediction, estimation of dynamical and mechanical stability of the monoclinic (space group $P2_1$) crystal, topological analysis of electron density, band structure and spectral (IR, Raman, UV, NMR) characterization as well as detonation and propulsive properties calculation. The modeling of both the crystalline and amorphous phases reveals high enthalpies of formation and densities. Detonation and propulsive properties of CarNit4 as a single explosive are close to that of hexahydro-1,3,5-trinitro-1,3,5-triazine (RDX). However, mixing of CarNit4 with oxidants (gaseous O_2) improves sharply the propulsive properties which become much higher than that of RDX. The same effect on detonation velocity and pressure is expected for formulations of CarNit4 with various positive oxygen balance explosives. Decomposition of CarNit4 in the presence of O_2 demonstrates the highest propulsive parameters under oxidation to carbon monoxide rather than carbon dioxide.

1. Introduction

Tetrazoles form a core of synthetic heterocyclic compounds, which are not found in nature. The synthesis of the tetrazole ring was first performed in far 1885 and now these molecules and their derivatives occupy a very important place in our life. The tetrazole ring is present in a number of drugs because its possesses bioisosterism to carboxylic acid and amide moieties, metabolic stability, etc. [1,2]. Apart of the pharmaceutical applications, tetrazoles are also used as components of polymer membranes in fuel cells, nanomaterials, catalysts and corrosion inhibitors [3].

Another very important area of application of tetrazoles is energetic materials [4]. Upon detachment of a proton, tetraloze formed a strongly aromatic tetrazolate anion, which can form salts with a number of cations [4] including transition metals [5]. At the same time, the N4 atom can accept a proton to form an onium (tetrazolium) cation. The latter also forms salts with various anions. Such reactivity enables a great variety of tetrazole energetic salts to be effectively synthesized for the last decade [4]. Tetrazolate anion can be oxidized to form 1N- and 2N-oxides, which are also applied as components of energetic salts [6].

When tetrazole or its N-oxides are coupled via the C5 atoms, a new class of energetic materials is obtained. Chart 1 demonstrates four examples of such compounds, but the other combinations of tetrazole and/or its N-oxide are also possible [7–14]. Meanwhile, one salt is of particular interest of researches among the great variety of such energetic compounds; this is dihydroxylammonium 5,5′-bistetrazole-1,1′-diolate (TKX-50) [15]. This compound demonstrates enhanced detonation properties and response to external energetic perturbations compared to the commonly used explosive materials [15]. Theoretical aspects of the decomposition mechanisms of TKX-50 and the related salts is briefly reviewed in our recent paper [16].

Such nitrogen-rich salts have a number of advantages compared to the organo-nitro explosives [17]. At first, this is enhanced detonation and propulsive performance, including specific impulse, flame temperature, etc. Secondly, the environmental safety is much better due to the inert gaseous products formed [17]. The latter reason is the driving force for researchers to discover compounds with even higher nitrogen content. In this regard, the most promising compounds are salts of cyclo-pentazolate N_5^- anion [18–20]. For many years, this species remained to be elusive structure, but now a simple versatile method for preparation of cyclo-pentazolate salts with a number of cations is presented [21]. Obviously, the highest nitrogen content is in pure allotropes of nitrogen [22–24], but now these structures are only hypothetical and, with rare exceptions [25], are not yet synthesized.

It is known that tetrazoles bearing an unsaturated moiety as a ring substituent can polymerize to form energetic polymers [26,27]. These

E-mail addresses: bondchem@cdu.edu.ua, bondchem@cdu.edu.ua.

https://doi.org/10.1016/j.polymer.2019.122048
Received 29 August 2019; Received in revised form 24 November 2019; Accepted 2 December 2019
Available online 6 December 2019
0032-3861/

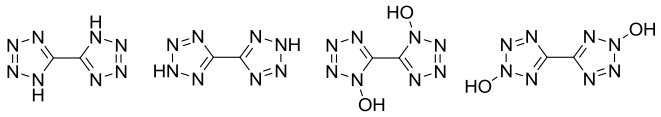

Chart 1. Several compounds with 5,5′-bistetrazole backbone.

polymers are usually insensitive to various external stimuli (impact, electric discharge, friction, etc.) and had a very good thermal stability [27]. The unsaturated moiety (say, a vinyl radical) can be bound to both the carbon and nitrogen atoms; as a result, one can find poly-5- and poly-1-vinyltetrazole, respectively [26]. As we have mentioned above, due to acidity of hydrogen at the N1 atom, the polymeric tetrazoles can form onium salts with typical n-nucleophiles. We should stress, however, that we are not familiar with any polymers bearing tetrazole units not as the side groups. In the present paper, we have predicted and characterized a new type of tetrazole-containing polymer built on the 1,5-tetrazolediyl fragments. Such structure has benefits of both a strong covalently-bound solid and highly energetic explosophore.

Recently, we have found that insertion of the carbon atoms into a pure nitrogen backbone significantly improves dynamical and mechanical stability of the latter [28,29]. With CN stoichiometry, such structures form very hard carbon nitrides. But what happens if the stoichiometry will change to CN_4? In this case, the nitrogen content will exceed most of the above-mentioned tetrazole salts (82.35 wt%). Thus, the results of such structure search and characterization are described below.

2. Computational details

In this work we performed first-principles calculations within the generalized gradient approximation (GGA) using Materials Studio 7.0 suite of programs [30]. Geometry optimizations, band structure (BS), phonons and vibrational spectra as well as optical properties calculations were done with Cambridge Serial Total Energy Package (CASTEP) code [31]. Elastic constants were obtained using DMol^3 code [32]. The functional due to Perdew-Burke-Ernzerhof (PBE) [33] was utilized entirely, except of BS and heat of formation (HOF) calculations. For these purposes we have applied hybrid functional, namely, HSE06 [34]. Compared to pure GGA functionals, the latter method was found to provide better performance in prediction of band gaps [35,36]. However, the accuracy of different functionals is a cornerstone of DFT and must be the issue of a separate study.

All the CASTEP calculations were performed with norm-conserving pseudopotentials (NCP) allowing correct description of the electron-core interactions. The electronic wave functions were expanded in a plane wave basis set with an energy cutoff equals 800 eV (58.8 Ry). Recently, we have shown this approach to be reliable for description of various tetrazole-based crystals [37]. The DMol^3 calculations were performed using all-electron approximation and a triple numerical basis set TNP [32]. Sampling of the Brillouin zone was performed using *k*-point mesh generated by the Monkhorst-Pack algorithm. Separation of *k*-points was specified to be 0.08 Å^{-1} for all the calculations, except of BS, optical properties, electron transitions and elastic constant calculations. In these cases the tightness of *k*-points was set to be 0.05 Å^{-1}. Convergence criteria of the total energy were specified to 5×10^{-6} eV atom^{-1} in the SCF calculations and 1×10^{-6} eV atom^{-1} during the fixed geometry calculations. For GGA/PBE approach the long-range effects were taken into account entirely using the Grimme form of the damped C_6 term [38]. Time-dependent DFT (TD-DFT) calculations were performed using the Tamm-Dankoff approximation [39].

To perform the Quantum Theory of Atoms in Molecules (QTAIM) analysis, wavefunctions were obtained using the projector augmented wave based method (PAW) [40]. This calculation was performed using the Quantum Espresso 5.3.0 program package [41]. Topological analysis of the electron density was done by means of the Critic2 software [42].

To model the amorphous state, a hydrogen terminated polymer (fifty 1,5-tetrazolediyl units) was constructed. Thereafter, the Amorphous Cell module of the Materials Studio 7.0 suite was applied to perform molecular dynamics modeling. A cubic supercell ($V = 47103.5$ Å^3, $\rho = 1.2$ g cm^{-3}) containing two polymer units (total number of atoms is 504) was then completely relaxed using Condensed-phase Optimized Molecular Potentials for Atomistic Simulation Studies (COMPASS) forcefield [43] within the Forcite module of the Materials Studio 7.0 [30]. Further, the supercell was relaxed using Density Functional based Tight Binding method (DFTB+, version 1.3) [44] as part of the Materials Studio 7.0 program suite [30]. The second-order energy expression involving self-consistent charge (SCC-DFTB) approximation with the Slater-Koster library MIO and with the empirical correction for van der Waals interactions was applied [31].

3. Results and discussion

3.1. Structural features and topological analysis

The crystal structure prediction reported here was performed with a CN_4 unit as a separate molecule. The latter can be either a diradical (Chart 2a) or a biradical (Chart 2b-c).

In the present work, a biradical (Chart 2b) appeared to be a monomeric unit of the studied polymer (Chart 2d). The crystal structure predicted in this work was obtained using our modified eigenvector-following scheme (Fig. S1 in the ESI). This method, allows to avoid optimization of hundreds or thousands of crystal structures, often very odd or improbable (like in the purely automatic algorithms), and restrict the number of structures to just a few. Of course, it does not guarantee that the resulting crystal will be the most thermodynamically stable polymorph (however, this cannot be excluded too). In the present work, our primary goal was to find possible structure, which is dynamically and mechanically stable at ambient conditions, and to estimate its density and enthalpy of formation.

If one assume that the crystal obtained this way is a metastable phase of poly(1,5-tetrazolediyl), this means that another stable polymorph does definitely exist. Meanwhile, Nyman and Day showed that for majority of organic crystals energy separation between polymorphs does not exceed 2 kJ mol^{-1} and the difference between their densities is about 0–2% [45]. A similar result we have recently obtained for crystal structure prediction of benzene diazonium chloride using Polymorph predictor [46]. As we will discuss below, such deviation causes very small effect on the resulting values of detonation velocity and pressure; therefore, one can neglect possible difference between polymorphs when calculating detonation properties. We should stress, however, that the true crystal structure is a crucial matter for estimation of explosives' sensitivity.

Thus, we have called the obtained polymer CarNit4 due to its stoichiometry as beginnings of the elements names (CN_4). The optimized asymmetric cell of CarNit4 is illustrated in Fig. 1a–d.

In crystalline state, CarNit4 has a monoclinic crystal system of the $P2_1$ space group. The other possible orthorhombic space group ($Cmc2_1$) is dynamically unstable due to the planar arrangement of the tetrazole rings. In the $P2_1$ space group crustal, these rings are out of plane by 21.3° (Fig. 1b). Therefore, the polymeric chains form zigzag alignment in perpendicular direction along the *a* axis (Fig. S2c in the ESI). The separate chains are clearly seen along the *b* axis (Fig. S2d in the ESI).

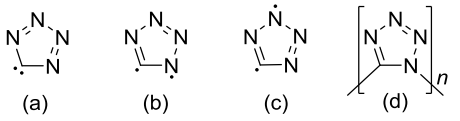

Chart 2. Possible arrangement of two unpaired electrons in a CN_4 residue.

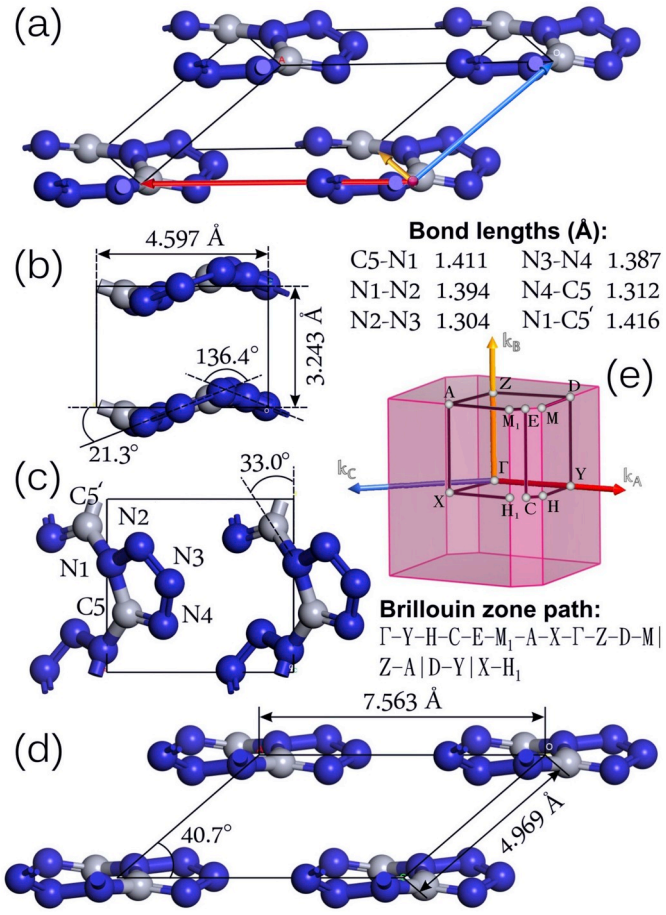

Fig. 1. Structural parameters at different projections of a CarNit4 unit cell (a–d); the Brillouin zone along with the corresponding high symmetry points (e).

To find out the interaction energy between the polymeric chains, we have performed a QTAIM analysis of the electron density distribution inside the asymmetric cell. The positions of all the bond (3, −1), ring (3, 1) and cage (3, 3) critical points (CPs) are shown in Fig. 2 and their fractional coordinates are listed in Table S1 in the ESI. The numerical values of electron density $\rho(\mathbf{r})$, its Laplacian $\nabla^2\rho(\mathbf{r})$ and potential energy density $v(\mathbf{r})$ are listed in Table 1. The latter values were calculated from the first two quantities using the Abramov gradient expansion (eq (1)) [47].

$$v(\mathbf{r}) = -\frac{3}{5}\left(3\pi^2\right)^{2/3}\rho(\mathbf{r})^{5/3} - \frac{1}{12}\nabla^2\rho(\mathbf{r}) \quad (1)$$

As one can see in Fig. 2, all the critical points (except of 4–10 and 17–18) characterize interactions between the polymeric chains. This also reflects in smaller values of the electron density (Table 1). It is known, that the energy of weak bonding can be simply estimated by means of the Espinoza formula (eq (2)) [48]:

$$E = 1/2v(\mathbf{r}) \quad (2)$$

Thus, taking into account the total potential energy density value and eq (2), the total energy of interaction between the polymeric chains is 50.9 kJ cell^{-1}.

Table 1
The calculated QTAIM parameters (in a. u.) for an asymmetric cell of CarNit4.

CP	Type	ρ(r)	$\nabla^2\rho$(r)	v(r)
1	(3,-1)	0.0049785	0.0163421	−0.00219539
2	(3,-1)	0.0077029	0.0251848	−0.00382400
3	(3,-1)	0.0078917	0.0259849	−0.00396173
4	(3,-1)	0.0178884	0.0627999	−0.01225950
5	(3,-1)	0.2274540	0.0427942	−0.49026008
6	(3,-1)	0.2312330	0.0403498	−0.50360772
7	(3,-1)	0.2733410	−0.1819290	−0.64595053
8	(3,-1)	0.2771770	0.4064530	−0.71051771
9	(3,-1)	0.2802110	0.3987220	−0.72226282
10	(3,-1)	0.3338190	0.2830580	−0.94605698
11	(3,1)	0.0021809	0.0063296	−0.00073809
12	(3,1)	0.0022257	0.0063510	−0.00074713
13	(3,1)	0.0026180	0.0076398	−0.00092222
14	(3,1)	0.0030230	0.0094419	−0.00114976
15	(3,1)	0.0044237	0.0136275	−0.00182018
16	(3,1)	0.0047218	0.0146153	−0.00198110
17	(3,1)	0.0147645	0.0477882	−0.00908502
18	(3,1)	0.0863407	0.2852110	−0.12062344
19	(3,3)	0.0020097	0.0058634	−0.00067240
20	(3,3)	0.0020694	0.0058147	−0.00067754
21	(3,3)	0.0020710	0.0058903	−0.00068409

3.2. Stability criteria

To be accepted as a stable crystal, it must satisfy at least dynamical and mechanical stability criteria. Dynamical stability is determined by the absence of soft modes in phonon spectrum; thus, we have performed phonon dispersion calculations. The Brillouin zone integration path was specified in accord with the standardized approach for each of the 24 Brillouin zones within 14 Bravais lattices [49]. For an MCL lattice the corresponding path is illustrated in Fig. 1e and the coordinates of high symmetry points are listed in Table S2 in the ESI [49]. The calculated phonon dispersion along with the density of phonon states is presented in Fig. 3. As it follows from Fig. 3, CarNit4 is dynamically stable due to the absence of soft modes. Also, the highest frequencies are more than 1400 cm^{-1} suggesting strong covalent bonds formed.

Meanwhile, the estimation of mechanical stability is a rather challenging task for such low-symmetry system as a monoclinic crystal. An MCL lattice has 13 independent elastic constants, which are presented in eq S(1) and the numerical values of constants C_{ij} and S_{ij} are listed in Tables S3 and S4 in the ESI. It is known that a necessary and sufficient condition of the mechanical stability of an MCL lattice is positive definiteness of the matrix S1. Algebraically, this can be expressed via the six

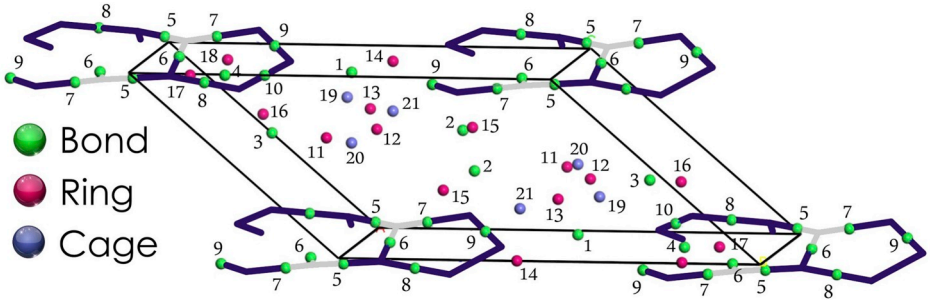

Fig. 2. Positions and type of the critical points in an asymmetric cell of CarNit4.

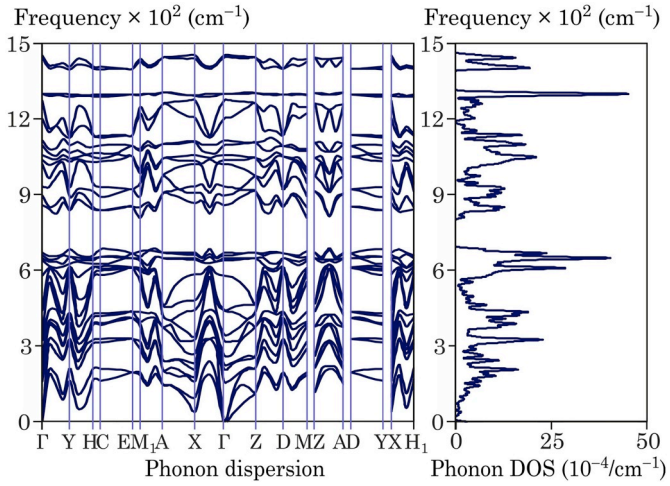

Fig. 3. Zero-pressure phonon dispersion and density of phonon states of CarNit4.

conditions in eq (3) [50]:

$$\begin{cases} C_{11} > 0 \\ C_{44} > 0 \\ C_{11}C_{22} - C_{12}^2 > 0 \\ C_{44}C_{66} - C_{46}^2 > 0 \\ T = C_{11}C_{22}C_{33} + 2C_{12}C_{13}C_{23} - C_{11}C_{23}^2 - C_{22}C_{13}^2 - C_{33}C_{12}^2 > 0 \\ C_{15}^2(C_{23}^2 - C_{22}C_{33}) + C_{25}^2(C_{13}^2 - C_{11}C_{33}) + C_{35}^2(C_{12}^2 - C_{11}C_{22}) \\ +2C_{15}C_{35}(C_{13}C_{22} - C_{12}C_{23}) + 2C_{15}C_{25}(C_{12}C_{33} - C_{13}C_{23}) \\ +2C_{25}C_{35}(C_{23}C_{11} - C_{12}C_{13}) + C_{55}T > 0 \end{cases} \quad (3)$$

Even such simple relations (eq (3)) take much time and efforts to be checked. If one performs a crystal structure prediction, the problem becomes much more acute since this procedure may be repeated many times. Therefore, we have developed a simple Pascal ABC.NET code, which checks the corresponding Born-Huang criteria [51] for a given Laue class. If the crystal satisfies the mechanical stability criteria and the corresponding elastic compliance matrix (in GPa^{-1}) is presented in the input file, a MatLab script is generated for plotting 3D map of the Young's modulus.

The corresponding equations are taken from ref [52]. For an MCL lattice this is the following (eq (4)).

$$\frac{1}{E} = l_1^4 s_{11} + 2l_1^2 l_2^2 s_{12} + 2l_1^2 l_3^2 s_{13} + 2l_1^3 l_3 s_{15} + l_2^4 s_{22} + 2l_2^2 l_3^2 s_{23} + 2l_1 l_2^2 l_3 s_{25} + l_3^4 s_{33} + 2l_1 l_3^3 s_{35} + l_2^2 l_3^2 s_{44} + 2l_1 l_2^2 l_3 s_{46} + l_1^2 l_3^2 s_{55} + l_1^2 l_2^2 s_{66} \quad (4)$$

herein, $l_1 = \sin\theta\cos\phi$, $l_2 = \sin\theta\sin\phi$ and $l_3 = \cos\theta$ are the directional cosines of angles with the three principal directions. As it follows form eq (3) and Table S3, CarNit4 is mechanically stable material at zero-pressure. The plotted 3D map of the Young's modulus is illustrated in Fig. 4 and the numerical values along with the Poisson ratios are listed in Table 2. The calculated bulk modulus is 22.3 GPa, while along the *y* axis, the Young's modulus reaches 139.3 GPa revealing a good mechanical strength of CarNit4.

3.3. Electronic and spectral properties

This section describes a series of calculations of spectral properties in order to provide data for further experimental identification of CarNit4 and for estimation of thermodynamic properties. The calculated electronic band structure and partial density of states plots of CarNit4, illustrated in Fig. S3 in the ESI,demonstrates an indirect bandgap ($\Gamma \rightarrow Y$) of 4.203 eV wide. Taking into account underestimation of band gaps by HSE06 functional (*ca.* 0.24 eV) [35], the obtained polymer is rather insulator than a wide bandgap semiconductor.

Additionally, we have calculated vibrational spectra of CarNit4. The infrared (IR) and Raman spectra are plotted in Fig. 5 and the tabulated data along with the corresponding eigenvectors are presented in Table S5 and Fig. S4 in the ESI. Due to the relatively low symmetry of CarNit4, a number of normal modes have non-zero intensities and both the IR and Raman spectra are informative. In Fig. 5, we have compared the calculated spectra for CarNit4 with experimental spectra of 1*H*-tetrazole [53,54]. Remarkably, we have an excellent agreement on the frequencies of the tetrazole bands in CarNit4; the difference is often a few cm^{-1} (Fig. 5).

It is interesting that mode 1452 cm^{-1} (ν_{C-N}) in 1*H*-tetrazole [54] is transformed into mode 1451 cm^{-1} (ν_{C-N}) in CarNit4, where C and N atoms belong to different tetrazole moieties. This is valence vibration of

Table 2
Young's modulus (*E*, GPa) and Poisson ratios (*ν*) of CarNit4.

Axis	*E* (GPa)	Poisson Ratios (*ν*)			
x	69.3	E_{xy}	0.0898	E_{xz}	1.2802
y	139.3	E_{yx}	0.1806	E_{yz}	0.4362
z	14.5	E_{zx}	0.2678	E_{zy}	0.0454

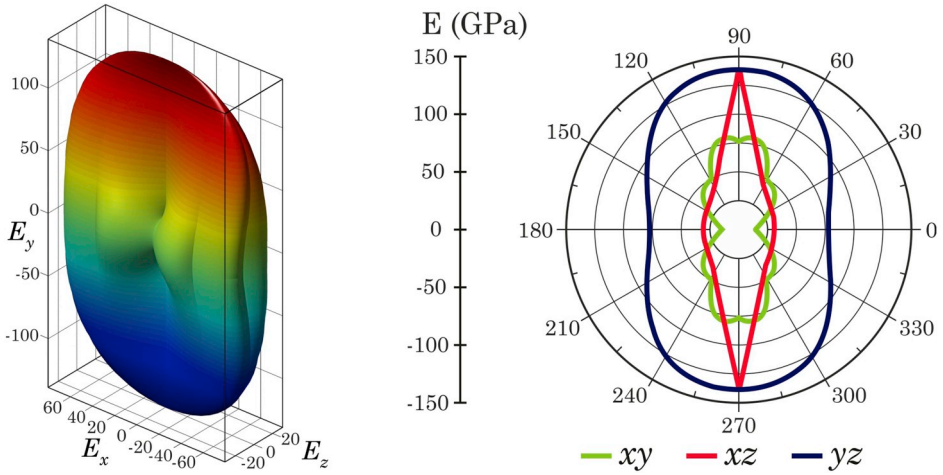

Fig. 4. The 3D plot of Young's modulus of CarNit4 together with the three projections on secant planes.

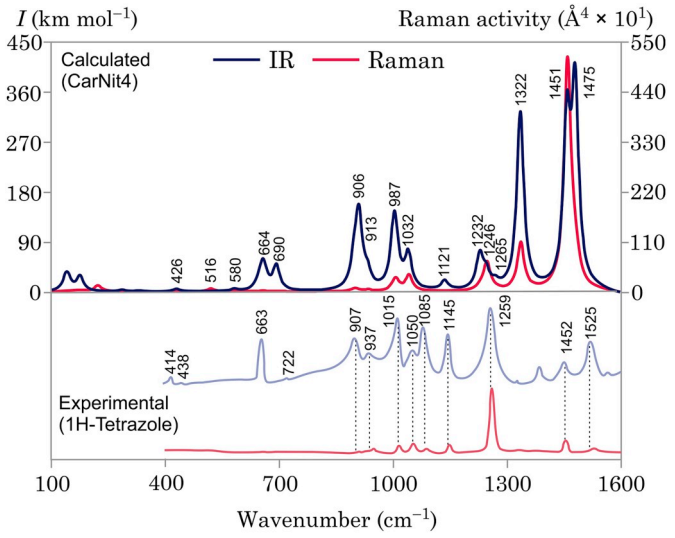

Fig. 5. The calculated IR and Raman spectra of CarNit4.

the formed C–N bond. Instead, a new band appears in the CarNit4 spectrum (mode 1322 cm^{-1}), which is the C–N1 bond valence vibration. Another change in the spectral picture is mode 1525 cm^{-1} ($\nu_{C=N}$) [54]. In CarNit4, this vibration appears with slightly lower frequency (mode 1475 cm^{-1}), but it is directly related to the C–N bond between the tetrazole rings (Fig. S4 in the ESI). The other vibrational modes in the IR spectrum of CarNit4 are directly related to the corresponding modes of 1*H*-tetrazole (Fig. 5). In the Raman spectrum of CarNit4, the main change is a sharp increasing of intensity of mode 1451 cm^{-1} (ν_{C-N}), which becomes the most active band (4602 $Å^4$). The new mode 1322 cm^{-1} also has relatively high activity (1384 $Å^4$). Finally, several low-frequency bands, modes 580 and 516 cm^{-1} (δ_{NCN}), appear in the Raman spectrum of CarNit4 (Fig. 5).

Apart of the vibrational spectra, we have calculated absorption spectrum of CarNit4 (Fig. 6). The other optical properties, including reflectivity, refractive index, dielectric function, conductivity and loss function, are presented in Fig. S5 in the ESI. To assign the absorption bands in the spectrum, we have performed TD-DFT calculations. The numerical data on the first eight transitions are gathered in Table 3 and the data on the transitions S_9–S_{20} are listed in Table S6 in the ESI. As one can see in Table 3, the TD-DFT calculations are in a complete agreement with the band structure. The first five excitations correspond to various transitions from a series of five valence bands (VB) to the conduction

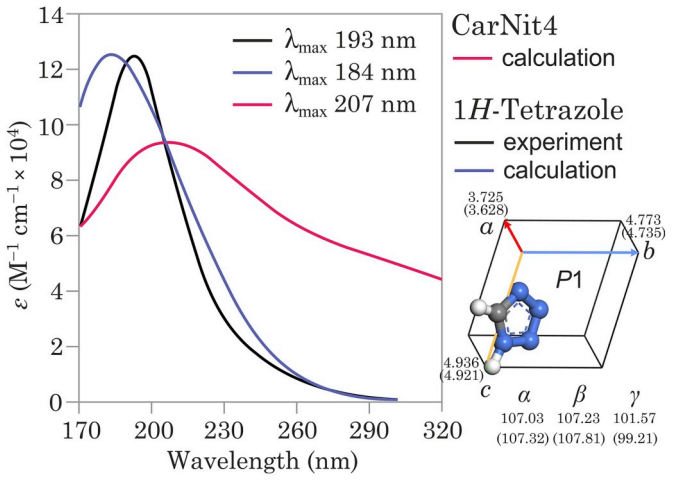

Fig. 6. The calculated absorption spectrum of CarNit4 in comparison to the 1H-tetrazole spectra. Inset represents crystal structure of 1H-tetrazole.

Table 3
Energies (eV) and orbital assignment of the first eight electron transitions in absorption spectrum of CarNit4.

State	*E* (eV)	Assignment	Overlap
S_1	4.633 (268 nm)	VB→CB	0.982182
S_2	4.763 (260 nm)	VB-1→CB	0.992660
S_3	5.175 (240 nm)	VB-2→CB	0.918438
S_4	5.705 (217 nm)	VB-4→CB	0.964436
S_5	5.734 (216 nm)	VB-3→CB	0.892713
S_6	6.481 (191 nm)	VB→CB+1	0.904278
S_7	6.578 (188 nm)	VB-1→CB+1	0.941822
S_8	6.889 (180 nm)	VB-5→CB	0.653050
		VB-2→CB+1	0.133526

band (CB). The next series of electronic transitions (S_5–S_8) includes excitations to the CB and CB+1 (Table 3). Note the corresponding crystal orbitals are illustrated in Fig. S6 in the ESI.

Using instrumental smearing 0.5 eV, we have obtained a single absorption band with λ_{max} 207 nm (Fig. 6). To check the reliability of our method of calculation, we have modeled the UV spectrum of 1*H*-tetrazole. It is known that the latter has a single absorption band with λ_{max} 193 nm at ambient conditions [55]. Remarkably, despite the C_S point group symmetry, 1*H*-tetrazole crystalizes in a very rare triclinic space group *P*1 [56]. According to the Cambridge Crystallographic Data Centre (CCDC) space group statistics, this space group has only 1% of entries [57]. Thus, we have completely optimized an asymmetric cell of 1*H*-tetrazole and obtain an excellent agreement on the lattice parameters (Fig. 6). Again, the calculated absorption spectrum of 1*H*-tetrazole is a very good agreement with experiment (λ_{max} 184 nm). Thus, we can conclude that our spectral data are reliable.

Finally, we have also used the gauge-including projector augmented-wave method (GIPAW) [58] in order to obtain chemical shielding and electric field gradient tensors. The calculated data are listed in Table S7 in the ESI.

3.4. Thermodynamic, detonation and propulsive properties

In order to estimate detonation and propulsive properties of CarNit4, we have obtained the temperature dependence of main thermodynamic functions, enthalpy (*H*), Gibbs free energy (*G*), entropy (*S*) and isobaric heat capacity (C_p) in the temperature range 0–5000 K. These results, along with the Debye temperature, are presented graphically in Fig. S7 in the ESI. The calculation of enthalpy of formation may become critical because of a wide variety of the values predicted. Thus, the values of ΔH_f^0, predicted with a set of pure GGA functionals (along with B3LYP) are listed in Table S8 in the ESI. These calculations were done using eq (5) [59]:

$$\Delta H_f^0 = 1/2E_{CarNit4} - 2E_{N_2} - 1/4E_{graphite} \quad (5)$$

where $E_{CarNit4}$, E_{N_2} and $E_{graphite}$ are the total energies of CarNit4, an isolated nitrogen molecule and graphite, respectively.

As it follows from Table S8, the values of ΔH_f^0 are all high but very different. Thus, we have decided to apply more accurate hybrid functional HSE06 which gives the value of ΔH_f^0 equals 375.9 kJ mol^{-1}. In addition to the crystalline form of CarNit4, we have modeled this material in amorphous state; our model is illustrated in Fig. 7. The calculation of ΔH_f^0 was performed according to eq (6), where E_{amorph}, E_{N_2}, E_{H_2} and $E_{graphite}$ are the corresponding DFTB energies. The coefficient *a* is obtained using the calculations of CarNit4 in the crystalline form as $a = \Delta H_{f(HSE06)}^0/\Delta H_{f(DFTB)}^0 = 1.969$.

$$\Delta H_f^0 = \frac{a}{100}\left(E_{amorph} - 200E_{N_2} - 2E_{H_2} - 25E_{graphite}\right) \quad (6)$$

Thus, the calculated value of ΔH_f^0 for the amorphous phase is 380.2

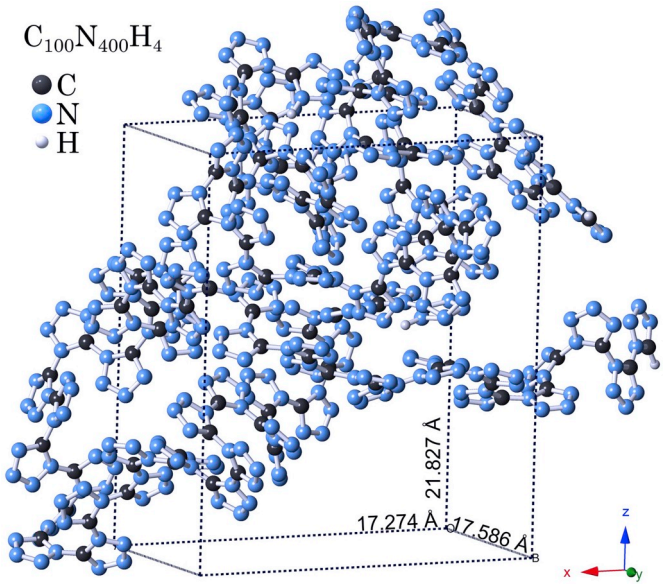

Fig. 7. The optimized supercell with two hydrogen terminated polymeric chains of poly(1,5-tetrazolediyl).

kJ mol^{-1}. In this work, we have applied the Kamlet-Jacobs (K-J) empirical equations (eqs (7) and (8)) to obtain detonation velocity (D, km s^{-1}) and pressure (P, GPa) [60]:

$$D = 1.01\left(N\overline{M}^{1/2}Q^{1/2}\right)^{1/2}(1 + 1.30\rho_0) \quad (7)$$

$$P = 1.558\rho_0^2 N\overline{M}^{1/2}Q^{1/2} \quad (8)$$

where N and $\overline{M}$ are the dimensionless structure specific parameters and Q is the detonation energy (cal g^{-1}). For a CarNit4 unit CN_4, the appropriate structural criterion is $2a + b/2 > d \geq b/2$; hence, these parameters are defined as the following [60]:

$$N = \frac{b + 2c + 2d}{4MW} \quad (9)$$

$$\overline{M} = \frac{56c + 88d - 8b}{b + 2c + 2d} \quad (10)$$

$$Q = \frac{\left[28.9b + 94.05(d/2 - b/4) + 239\Delta H_f^0\right]}{MW} \quad (11)$$

where, a, b, c and d are the number of carbon, hydrogen, nitrogen and oxygen atoms, respectively; MW is the molecular weight.

The calculated parameters Q, D and P along with the corresponding densities for crystalline and amorphous phases are listed in Table 4. The same values for hexahydro-1,3,5-trinitro-1,3,5-triazine (RDX) calculated using eqs (7) and (8) are the following: D (35.21 km s^{-1}) and P (8.88 GPa). Thus, as it follows from Table 5, the crystalline form of CarNit4 has detonation performance comparable to that of RDX. We should stress, however, that CarNit4 suffers from a lack of internal oxidizer (oxygen balance −47.0%). A simple mixture of CarNit4 with any positive oxygen balance explosive will improve the detonation parameters sharply. For example, if we add an oxygen atom to the CarNit4 formula unit (CN_4O) and assume that enthalpy and density remain the same, the Q, D and P values become 1628.6 cal g^{-1}, 9.43 km s^{-1} and 42.00 GPa, respectively. At the same time, CarNit4 is a nitrogen-rich material and has a significant advantage compared to RDX, since the main detonation product is environmental friendly molecular nitrogen.

Table 4
The calculated detonation properties of CarNit4.

Phase	ρ (g cm^3)	Q	D	P
$P2_1$	2.005	1320.4	35.40	8.65
amorph.	1.717	1335.5	26.11	7.78

Table 5
The calculated propulsive properties of CarNit4 as monopropellant (O/F = 0) and in a mixture with O_2 (O/F ≠ 0) at 300 K.

O/F	CCT	M^a	I_{sp}	I_{vac}	c^*
0	3502	34.0	257	281	1525
0.23516	4763	28.0	300	319	1843
0.47031	3590	30.3	273	299	1639

[a] Molecular weight of the reaction products.

As we have mentioned above, the possible difference of the ρ and ΔH_f^0 values between polymorphs can be neglected when estimating detonation properties. For example, for the α- and β-polymorphs of hexahydro-1,3,5-trinitro-1,3,5-triazine (RDX) the difference between ρ and ΔH_f^0 are the following: 0.014 g cm^{-3} [61] and 0.6 kJ mol^{-1} [62]. Taking into account such small difference, the resulting detonation properties (Q, P and D) calculated using the K-J scheme are the following: 1500.9 cal g^{-1}, 8.83 km s^{-1} and 34.7 GPa versus 1501.6 cal g^{-1}, 8.88 km s^{-1} and 35.3 GPa for α- and β-polymorphs, respectively. We should stress that the K-J empirical scheme is a well-established method for prediction of detonation properties and, as we have shown in our recent paper [63], it outperforms in accuracy the most recent predictors, like EMDB, EXPLO5 and Cheetah 8.0.

Finally, we have estimated propulsive properties of CarNit4. For this purpose, we have first converted the CASTEP thermodynamic properties (Fig. S7 in the ESI) to the NASA 9 coefficients form [64] using our previously described code i97creator [63] and the PAC99 routine. Thereafter, the propulsive properties, namely, combustion chamber temperature (CCT, K), specific impulse (I_{sp}, s), vacuum specific impulse (I_{vac}, s) and characteristic velocity (c^*, m s^{-1}), were calculated with NASA CEA2 program [65]. The obtained propulsive properties are listed in Table 5 and the NASA coefficients for CarNit4 are presented in the ESI.

Being used as a monopropellant (oxidant-to-fuel weight ratio O/F = 0), CarNit4 decomposes to the following equation:

$$CN_{4(s)} \rightarrow C_{(s)} + 2N_{2(g)}$$

The corresponding mole fractions of decomposition products for various exit-to-throat area ratios (Ae/At) are presented in Table S9 in the ESI. As one can see in Table 5, CarNit4 has slightly poorer propulsive performance compared to RDX (I_{sp} = 268 s) [66]. Nevertheless, when an oxidant (say, gaseous O_2) is added, the propulsive properties significantly exceed those of RDX. As it follows from our calculations, the most effective weight ratio of O_2 and CarNit4 is O/F = 0.23516 that corresponds to the following equation (Tables 5 and S10 in the ESI):

$$0.5O_{2(g)} + CN_{4(s)} \rightarrow CO_{(g)} + 2N_{2(g)}$$

Addition of a more amount of oxidant leads to unexpected results. For example, if one assumes the complete oxidation of carbon to CO_2 (O/F = 0.47031), then the formation of a complex mixture of CO, CO_2, NO and unreacted O_2 will take place (Table S11 in the ESI). This also results in a lowering of the propulsive properties of the mixture (Table 5).

4. Conclusions

In summary, we have predicted crystal structure and performed a comprehensive theoretical study of a new polymeric material based on 1,5-tetrazolediyl units. This polymer is a nitrogen-rich material (82.35 wt%) with high energy density. Thus, the most probable area of application of CarNit4 is energetic materials. Indeed, in both the crystalline and amorphous state, CarNit4 has high enthalpies of formation and

crystal densities, which makes its detonation properties being close to the conventional explosives, like RDX. On the other hand, a lack of internal oxidant prevents demonstration of the highest potential of CarNit4 as energetic material. Thus, formulations of CarNit4 with positive oxygen balance explosives allow obtaining enhanced detonation performance of CarNit4 in comparison with conventional explosives. The same situation is expected when use CarNit4 as solid propellant. A simple addition of a half of mole of oxygen per mole of CarNit4 produces enhanced propulsive properties compared to RDX, which can also find its application in future.

We have found that insertion of carbon atoms into the nitrogen backbone significantly improves dynamical and mechanical stability [28,29]. Thus, one can obtain nitrogen-rich material bearing single- and double-bonded nitrogen. On the other hand, the presence of carbon in explosive materials is less desirable due to formation of carbon oxides. From this point of view the most potentially favorable energetic materials need to be inorganic carbon-free $H_xN_yO_z$ formulations. The recently synthesized, pentazolate *cyclo*-N_5^- salts are good examples of such materials [21]. The main detonation products in this case are environmental friendly substances. Thus, prediction and characterization of such compounds is of great practical interest and will be the issue for further studies.

Author contributions section

Sergey V. Bondarchuk: Conceptualization, Methodology, Software, Data curation, Writing-Original draft preparation, Visualization, Investigation, Writing-Reviewing and Editing.

Declaration of competing interest

The authors declare that they have no known competing financial interests or personal relationships that could have appeared to influence the work reported in this paper.

Acknowledgements

This work was supported by the Ministry of Education and Science of Ukraine, Research Fund (Grant No. 0118U003862).

Appendix A. Supplementary data

Supplementary data to this article can be found online at https://doi.org/10.1016/j.polymer.2019.122048.

References

[1] C.G. Neochoritis, T. Zhao, A. Dömling, Tetrazoles via multicomponent reactions, Chem. Rev. 119 (2019) 1970–2042.
[2] R. Varala, B. Hari Babu, A click chemistry approach to tetrazoles: recent advances, in: D. Vlachakis (Ed.), Molecular Docking, IntechOpen, London, 2018, pp. 51–75.
[3] V.A. Ostrovskii, E.A. Popova, R.E. Trifonov, Developments in tetrazole chemistry (2009-16), in: E. Scriven, Ch Ramsden (Eds.), Advances in Heterocyclic Chemistry, Academic Press, Oxford, 2017, pp. 1–62.
[4] H. Gao, J.M. Shreeve, Azole-based energetic salts, Chem. Rev. 111 (2011) 7377–7436.
[5] A. Rodríguez-Diéguez, E. Colacio, [Zn_n(polyox)(pmtz)$_n$]: the first polyoxalate-containing coordination polymer from an unforeseen chemical rearrangement of 5-pyrimidyltetrazole under hydrothermal conditions, Chem. Commun. (2006) 4140–4142.
[6] P. He, J.-G. Zhang, X. Yin, J.-T. Wu, L. Wu, Z.-N. Zhou, T.-L. Zhang, Energetic salts based on tetrazole N-oxide, Chem. Eur J. 22 (2016) 7670–7685.
[7] Y. Shang, B. Jin, R. Peng, Z. Guo, Q. Liu, J. Zhao, Q. Zhang, Nitrogen-rich energetic salts of 1H,1'H-5,5'-Bistetrazole-1,1'-diolate: synthesis, characterization, and thermal behaviors, RSC Adv. 6 (2016) 48590–48598.
[8] N. Fischer, T.M. Klapötke, K. Peters, M. Rusan, J. Stierstorfer, Alkaline earth metal salts of 5,5'-bistetrazole – from academical interest to practical application, Z. Anorg. Allg. Chem. 637 (2011) 1693–1701.
[9] P. He, L. Wu, J. Wu, Q. Wang, Z. Li, M. Gozin, J. Zhang, Green energetic nitrogen-rich salts of 1,1'-Dinitramino-5,5'-Bistetrazolate, Chem. Eur J. 23 (2017) 11159–11168.
[10] L.H. Finger, F.G. Schröder, J. Sundermeyer, Synthesis and characterisation of 5,5'-Bistetrazolate salts with alkali metal, ammonium and imidazolium cations, Z. Anorg. Allg. Chem. 639 (2013) 1140–1152.
[11] N. Fischer, T.M. Klapötke, M. Reymann, J. Stierstorfer, Nitrogen-rich salts of 1H,1'H-5,5'-Bitetrazole-1,1'-diol: energetic materials with high thermal stability, Eur. J. Inorg. Chem. 2013 (2013) 2167–2180.
[12] D. Fischer, T.M. Klapötke, J. Stierstorfer, N. Szimhardt, 1,1'-Nitramino-5,5'-bitetrazoles, Chem. Eur J. 22 (2016) 4966–4970.
[13] D. Fischer, T.M. Klapötke, M. Reymann, PhC. Schmid, J. Stierstorfer, M. Sućeska, Synthesis of 5-(1H-Tetrazolyl)-1-hydroxy-tetrazole and energetically relevant nitrogen-rich ionic derivatives, Propellants, Explos. Pyrotech. 35 (2010) 1–8.
[14] T.M. Klapötke, M.Q. Kurz, R. Scharf, PhC. Schmid, J. Stierstorfer, M. Sućeska, 5-(1H-Tetrazolyl)-2-Hydroxy-Tetrazole: a selective 2N-monoxidation of Bis(1H-tetrazole), ChemPlusChem 80 (2015) 97–106.
[15] N. Fischer, D. Fischer, T.M. Klapötke, D.J. Piercey, J. Stierstorfer, Pushing the limits of energetic materials – the synthesis and characterization of dihydroxylammonium 5,5'-bistetrazole-1,1'-diolate, J. Mater. Chem. 22 (2012) 20418–20422.
[16] S.V. Bondarchuk, in: J.A. Seijas Vázquez (Ed.), ECSOC-21, Proceedings of the 21st International Electronic Conference on Synthetic Organic Chemistry, 2017, https://doi.org/10.3390/ecsoc-21-04781. November 1-30.
[17] T.M. Klapötke, New nitrogen-rich high explosives, in: T.M. Klapötke (Ed.), High Energy Density Materials, Springer, Berlin, Heidelberg, 2007, pp. 85–121.
[18] P. Wang, Y. Xu, Q. Lin, M. Lu, Recent advances in the syntheses and properties of polynitrogen pentazolate anion cyclo-N_5^- and its derivatives, Chem. Soc. Rev. 47 (2018) 7522–7538.
[19] T. Yu, Y.-D. Ma, W.-P. Lai, Y.-Z. Liu, Z.-X. Ge, G. Ren, Roads to pentazolate anion: a theoretical insight, R. Soc. Open Sci. 5 (2018) 172269.
[20] Ch Zhang, Ch Sun, B. Hu, Ch Yu, M. Lu, Synthesis and characterization of the pentazolate anion cyclo-N_5^- in $(N_5)_6(H_3O)_3(NH_4)_4Cl$, Science 355 (2017) 374–376.
[21] Y. Xu, L. Tian, D. Li, P. Wang, M. Lu, A series of energetic cyclo-pentazolate salts: rapid synthesis, characterization, and promising performance, J. Mater. Chem. 7 (2019) 12468–12479.
[22] S.V. Bondarchuk, B.F. Minaev, Super high-energy density single-bonded trigonal nitrogen allotrope—a chemical twin of the cubic gauche form of nitrogen, Phys. Chem. Chem. Phys. 19 (2017) 6698–6706.
[23] S.V. Bondarchuk, B.F. Minaev, Two-dimensional honeycomb (A7) and zigzag sheet (ZS) type nitrogen monolayers. A first principles study of structural, electronic, spectral, and mechanical properties, Comput, Mater. Sci. 133 (2017) 122–129.
[24] S.V. Bondarchuk, Beyond molecular nitrogen: revelation of two ambient-pressure metastable single- and double-bonded nitrogen allotropes built from three-membered rings, Phys. Chem. Chem. Phys. 21 (2019) 22930–22938.
[25] M.I. Eremets, A.G. Gavriliuk, I.A. Trojan, D.A. Dzivenko, R. Boehler, Single-bonded cubic form of nitrogen, Nat. Mater. 3 (2004) 558–563.
[26] E. Pasquinet, Nitrogen-rich polymers as candidates for energetic applications, in: A. De Souza Gomes (Ed.), New Polymers for Special Applications, IntechOpen, London, 2012, pp. 313–338.
[27] F.M. Betzler, R. Boller, A. Grossmann, T.M. Klapötke, Novel insensitive energetic nitrogen-rich polymers based on tetrazoles, Z. Naturforschung 38b (2013) 714–718.
[28] S.V. Bondarchuk, B.F. Minaev, Two isomeric solid carbon nitrides with 1 : 1 stoichiometry which exhibit strong mechanical anisotropy, New J. Chem. 41 (2017) 13140–13148.
[29] S.V. Bondarchuk, B.F. Minaev, DFT design of polyguanidine – a unique two-dimensional material with high-energy density, Mol. Phys. 115 (2017) 2423–2430.
[30] Materials Studio 7.0, Accelrys, Inc., San Diego, CA, 2013.
[31] S.J. Clark, M.D. Segall, C.J. Pickard, P.J. Hasnip, M.J. Probert, K. Refson, M. C. Payne, First principles methods using CASTEP, Z. für Kristallogr. - Cryst. Mater. 220 (2005) 567–570.
[32] B. Delley, From molecules to solids with the DMol^3 approach, J. Chem. Phys. 113 (2000) 7756–7764.
[33] J.P. Perdew, K. Burke, M. Ernzerhof, Generalized gradient approximation made simple, Phys. Rev. Lett. 77 (1996) 3865–3868.
[34] J. Heyd, G. Scuseria, Efficient hybrid density functional calculations in solids: assessment of the Heyd-Scuseria-Ernzerhof screened Coulomb hybrid functional, J. Chem. Phys. 121 (2004) 1187–1192.
[35] A.J. Garza, G.E. Scuseria, Predicting band gaps with hybrid density functionals, J. Phys. Chem. Lett. 7 (2016) 4165–4170.
[36] G.M. Dongho Nguimdo, D.P. Joubert, A density functional (PBE, PBEsol, HSE06) study of the structural, electronic and optical properties of the ternary compounds $AgAlX_2$ (X = S, Se, Te), Eur. Phys. J. B 88 (2015) 113.
[37] S.V. Bondarchuk, Significance of crystal habit sphericity in the determination of the impact sensitivity of bistetrazole-based energetic salts, CrystEngComm 20 (2018) 5718–5725.
[38] S. Grimme, Semiempirical GGA-type density functional constructed with a long-range dispersion correction, J. Comput. Chem. 27 (2006) 1787–1799.
[39] S. Hirata, M. Head-Gordon, Time-dependent density functional theory within the Tamm-Dancoff approximation, Chem. Phys. Lett. 314 (1999) 291–299.
[40] G. Kresse, D. Joubert, From ultrasoft pseudopotentials to the projector augmented-wave method, Phys. Rev. B 59 (1999) 1758–1775.
[41] P. Giannozzi, S. Baroni, N. Bonini, M. Calandra, R. Car, C. Cavazzoni, D. Ceresoli, G.L. Chiarotti, M. Cococcioni, I. Dabo, A. Dal Corso, S. Fabris, G. Fratesi, S. de Gironcoli, R. Gebauer, U. Gerstmann, C. Gougoussis, A. Kokalj, M. Lazzeri, L. Martin-Samos, N. Marzari, F. Mauri, R. Mazzarello, S. Paolini, A. Pasquarello, L. Paulatto, C. Sbraccia, S. Scandolo, G. Sclauzero, A.P. Seitsonen, A. Smogunov, P. Umari, R.M. Wentzcovitch, J. Phys. Condens. Matter 21 (2009) 395502.

[42] A. Otero-De-La-Roza, E.R. Johnson, V. Luaña, Critic2: a program for real-space analysis of quantum chemical interactions in solids, Comput. Phys. Commun. 185 (2014) 1007–1018.
[43] H. Sun, COMPASS: an ab initio force-field optimized for condensed-phase Applications overview with details on alkane and benzene compounds, J. Phys. Chem. B 102 (1998) 7338–7364.
[44] T. Frauenheim, G. Seifert, M. Elstner, T. Niehaus, C. Köhler, M. Amkreutz, M. Sternberg, Z. Hajnal, A. Di Carlo, S. Suhai, Atomistic simulations of complex materials: ground-state and excited-state properties, J. Phys. Condens. Matter 14 (2005) 3015–3047.
[45] J. Nyman, G.M. Day, Static and lattice vibrational energy differences between polymorphs, CrystEngComm 17 (2015) 5154–5165.
[46] S.V. Bondarchuk, Impact sensitivity of aryl diazonium chlorides: limitations of molecular and solid-state approach, J. Mol. Graph. Model. 89 (2019) 114–121.
[47] YuA. Abramov, On the possibility of kinetic energy density evaluation from the experimental electron-density distribution, Acta Crystallogr. A53 (1997) 264–272.
[48] E. Espinosa, E. Molins, C. Lecomte, Hydrogen bond strengths revealed by topological analyses of experimentally observed electron densities, Chem. Phys. Lett. 285 (1998) 170–173.
[49] W. Setyawan, S. Curtarolo, High-throughput electronic band structure calculations: challenges and tools, Comput. Mater. Sci. 49 (2010) 299–312.
[50] M. Wen, X. Xie, Y. Gao, H. Dong, Z. Mu, F. Wu, C.-Y. Wang, Transition-metal-element dependence of ideal shear strength and elastic behaviors of γ′-Ni_3Al: ab initio study to guide rational alloy design, J. Alloy. Comp. 806 (2019) 1260–1266.
[51] F. Mouhat, F.-X. Coudert, Necessary and sufficient elastic stability conditions in various crystal systems, Phys. Rev. B 90 (2014) 224104.
[52] J.F. Nye, Physical Properties of Crystals: Their Representation by Tensors and Matrices, Oxford University Press Inc., Oxford, 1985.
[53] F. Billesa, H. Endrédi, G. Keresztury, Vibrational spectroscopy of triazoles and tetrazole, J. Mol. Struct.: THEOCHEM 530 (2000) 183–200.
[54] W. Li, X. Huang, K. Bao, Z. Zhao, Y. Huang, L. Wang, G. Wu, B. Zhou, D. Duan, F. Li, Q. Zhou, B. Liu, T. Cui, A novel high-density phase and amorphization of nitrogen-rich 1H-tetrazole (CH_2N_4) under high pressure, Sci. Rep. 7 (2017) 39249.
[55] Z. Sun, X.-Q. Zeng, W. Wang, M.-F. Ge, D.-X. Wang, Photoelectron spectroscopy and UV absorption spectroscopy studies on some nitrogen catenation compounds, Acta Chim. Sin. 64 (2006) 218–222.
[56] R. Goddard, O. Heinemann, C. Krüger, α-1H-1,2,3,4-Tetrazole, Acta Crystallogr. C53 (1997) 590–592.
[57] CSD space group statistics – space group number ordering. https://www.ccdc.cam.ac.uk/, 2019.
[58] C.J. Pickard, F. Mauri, All-electron magnetic response with pseudopotentials: NMR chemical shifts, Phys. Rev. B 63 (2001) 245101.
[59] E.N. Brothers, A.F. Izmaylov, A.A. Rusakov, G.E. Scuseria, On calculating a polymer's enthalpy of formation with quantum chemical methods, J. Phys. Chem. B 111 (2007) 13869–13872.
[60] M.J. Kamlet, S.J. Jacobs, Chemistry of detonations. I. A simple method for calculating detonation properties of C-H-N-O explosives, J. Chem. Phys. 48 (1968) 23–35.
[61] D.I.A. Millar, I.D.H. Oswald, D.J. Francis, W.G. Marshall, C.R. Pulham, A. S. Cumming, The crystal structure of β-RDX—an elusive form of an explosive revealed, Chem. Commun. (2009) 562–564.
[62] M. Ghosh, S. Banerjee, M.A.S. Khan, N. Sikdera, A.K. Sikder, Understanding metastable phase transformation during crystallization of RDX, HMX and CL-20: experimental and DFT studies, Phys. Chem. Chem. Phys. 18 (2016) 23554–23571.
[63] S.V. Bondarchuk, N.A. Yefimenko, An algorithm for evaluation of potential hazards in Research and development of new energetic materials in terms of their detonation and ballistic profiles, Propellants, Explos. Pyrotech. 43 (2018) 818–824.
[64] B.J. McBride, M.J. Zehe, S. Gordon, NASA Glenn Coefficients for Calculating Thermodynamic Properties of Individual Species, TP-2002-211556, NASA, Cleveland, OH, 2002.
[65] S. Gordon, B.J. McBride, Computer Program for Calculation of Complex Chemical Equilibrium Compositions and Applications. I. Analysis, NASA, Cleveland, OH, 1994. NASA Reference Publication 1311.
[66] T. Yu, B. Wu, A theoretical prediction on CN_6O: structure, stability and performance, Inorg. Chem. Front. 2 (2015) 991–1000.